



Article

A Hexagonal Bi-Isotropic Honeycomb in PCB †

Ismael Barba ^{1,*}, Óscar Fernández ², Álvaro Gómez-Gómez ², Ana Grande ¹ and Ana Cristina López-Cabeceira ¹

- Departamento de Electricidad y Electrónica, Universidad de Valladolid, 47011 Valladolid, Spain; anamaria.grande@uva.es (A.G.); anac.lopez@uva.es (A.C.L.-C.)
- Departamento de Ingeniería de Comunicaciones, Universidad de Cantabria, 39005 Santander, Spain; oscar.fernandez@unican.es (Ó.F.); alvaro.gomez@unican.es (Á.G.-G.)
- * Correspondence: ismael.barba@uva.es
- [†] This paper is an expanded version of Barba, I.; Grande, A.; López-Cabeceira, A.C.; Represa, J. A Bi-Isotropic Hexachiral Grid in PCB. In Proceedings of the IEEE MTT-S International Conference on Numerical Electromagnetic Modeling and Optimization for RF, Microwave, and Terahertz Applications—NEMO, Sevilla, Spain, 17–19 May 2017.

Abstract

In this study we explored the chiral behavior of a honeycomb-like chiral metamaterial with a negative Poisson's ratio. This type of structure is widely used in sectors such as construction and packaging, but is not as common in electromagnetics/electrical engineering. Moreover, in contrast with typical layer-by-layer chiral metamaterial structures, which are usually formed by metallic patterns with C4 symmetry, this hexachiral structure presents C6 symmetry. The aim of this paper is analyzing the electromagnetic behavior of this kind of auxetic metamaterial with special attention to its chiral behavior. This structure is analyzed by means of measurements and simulations of its reflection and transmission responses (scattering parameters) in different configurations, showing that a dual-layer configuration with conjugated faces provides high electromagnetic activity (gyrotropy) with low losses.

Keywords: electromagnetic activity; chiral media; cross polarization; bianisotropic media; metamaterials; polarization control; microwave propagation



Academic Editor: Giovanni Riccio

Received: 30 April 2025 Revised: 4 June 2025 Accepted: 18 June 2025 Published: 21 June 2025

Citation: Barba, I.; Fernández, Ó.; Gómez-Gómez, Á.; Grande, A.; López-Cabeceira, A.C. A Hexagonal Bi-Isotropic Honeycomb in PCB. *Electronics* **2025**, *14*, 2521. https://doi.org/10.3390/ electronics14132521

Copyright: © 2025 by the authors. Licensee MDPI, Basel, Switzerland. This article is an open access article distributed under the terms and conditions of the Creative Commons Attribution (CC BY) license (https://creativecommons.org/licenses/by/4.0/).

1. Introduction

The term "chirality" refers to a geometrical property: the lack of any mirror symmetry plane. Chiral geometries produce various electromagnetic, optical, or mechanical effects. From an electromagnetic perspective, they may lead to cross-coupling (bianisotropy) between the electric and magnetic fields for waves travelling inside them [1]. From a phenomenological perspective, these media feature electromagnetic/optical activity (gyrotropy, rotation of the polarization plane of a linearly polarized electromagnetic wave as it travels through these materials). Another consequence is the circular dichroism, i.e., the differential absorption of left-handed circularly polarized (LCP) and right-handed circularly polarized (RCP) waves. These properties have attracted much interest because of their potential applications in polarization control (rotators, circular polarizers, etc.) and also as a way to achieve negative refraction [1–18]

Unfortunately, these effects, consequences of the chiral geometry, are very weak and difficult to find at microwave frequencies [2]. To avoid these drawbacks, composite materials, usually composed of metals and dielectrics, can be engineered to achieve the desired properties, that is, metamaterials [3]. These properties have mainly been achieved by using periodic distributions of 3D geometrically chiral particles or 2D particles in bilayer

Electronics **2025**, 14, 2521 2 of 14

configurations [4–9]. These particles support chiral resonant modes rotating in the unit cell [7,10,11], which means that their maximum electromagnetic activity also tends to happen at the maximum of absorption. Sometimes, this may be a desired effect when working with absorption related properties (circular dichroism), for example, in linear-to-circular polarization converters [12]. Nevertheless, it involves high losses and dispersion and is undesired when we want to rotate the polarization plane with high transmission and low polarization distortion [5,11,13]. As an alternative, other approximations employ connected conductor fishnet-like patterns, usually complementary to "bulk" chiral media [10,14–17].

In addition, structures with six-fold symmetry (also known as "honeycombs") have been widely used in different sectors, such as aerospace, construction, and packaging, owing to their special featured properties (mechanical, optical, thermal, and electromagnetic) [18,19].

In 1989, Wojciechowski and Branca proposed a "tilted" honeycomb, with six-fold symmetry but no mirror symmetry in a plane (that is, chiral in a plane) to obtain a negative Poisson's ratio (see Figure 1) [20]. Other implications of geometrical chirality in terms of mechanical properties have been studied, including enhanced compressive strength capabilities, shear stiffness compared to classical centrosymmetric honeycomb configurations, synclastic curvature features, high indentation resistance, and high shear resistance [18–21]. These mechanical properties led David et al. to propose their application in electromagnetic absorbers, combining mechanical and electromagnetic behaviors into the same structure [22].

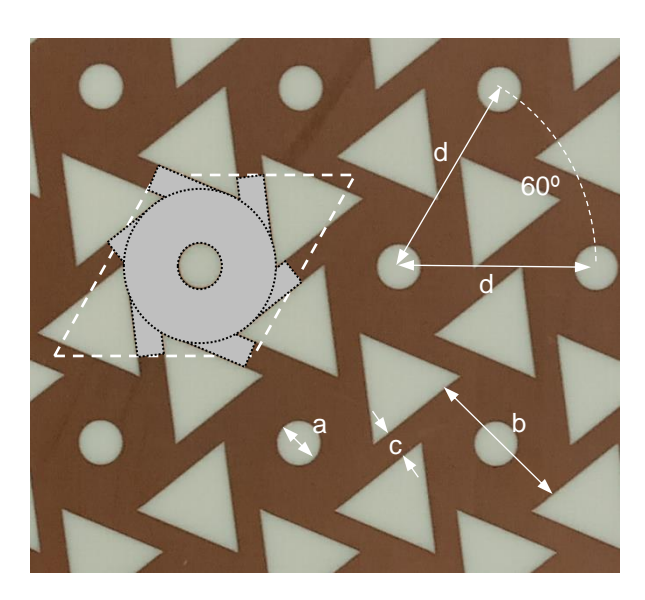


Figure 1. Manufactured hexachiral structure. The unit cell, delimited with a dash line, is formed by a circular crown of inner radius a and outer radius b, and six arms of width c tangent to the crown that interconnect with the neighbor elements distanced d. Please note that the structure can be rotated 60° without changing its appearance, i.e., it presents six-fold (C6) symmetry. The geometrical parameters of all the examples presented in this paper are a = 3.59 mm, b = 12.39 mm, c = 2.2 mm, and d = 16.48 mm.

In addition, Kopyt et al. studied the electromagnetic behavior of a structure implemented with lossy dielectrics (polymers) in 2010 to determine whether their structural chirality translates into chiral electromagnetic behavior (bianisotropy) [23], with negative results. It is worth noting that only a single layer of the structure was characterized in this study. Consequently, since the pattern is not geometrically chiral in the 3D space, no bi-anisotropic behavior should have been expected [4,24]. Although some "planar chiral" structures, with polarization conversion effects, have been found [25], it seems to be a

Electronics **2025**, 14, 2521 3 of 14

radically different phenomenon, with similarities to the well-known nonreciprocity of the Faraday effect in magnetized media. This "planar chirality" leads to a partial conversion of the incident wave into one of opposite handedness, the efficiency of this conversion being asymmetric for the opposite directions of propagation, while the gyrotropy in chiral media is completely symmetric for waves propagating in opposite directions [25]. Even more, this phenomenon requires the simultaneous presence of such "planar chirality" and anisotropy in the plane [26]. In the previous references, as well as the examples studied in this paper, all the structures are considered "isotropic" in the plane, so such behavior should not be present.

In this study, we designed and studied different configurations of the same hexachiral structure, with the aim of obtaining evidence of electromagnetic chiral behavior (gyrotropy) [1] with low dichroism and energy losses. Since in this paper we only study the electromagnetic properties of such structures, we use a metallic fishnet, using Printed Circuit Board (PCB) technology, so we have a connected conductor structure as mentioned above. Second, modification of the original planar structure is necessary to obtain a 3D chiral geometry. This may be achieved by means of a bilayer conjugated structure (easy to obtain metallizing both sides of the board) through electromagnetic coupling between the layers, when the geometry of one layer is the specular image of the other one's [13,17,27].

A first numerical result was published in a conference in 2017 [28], which found electromagnetic activity in a conjugated structure. Another numerical study of a geometrically similar structure was published in 2018 [29], though in this case the structure was full dielectric so the physical explanation of its behavior was different and not applicable here. Here, the origin of this behavior is studied by modelling several different structures based on the same honeycomb pattern that differs in the number of printed faces of the PCB and in the orientation of the pattern, as shown in Figure 2. Other interesting results, like extraordinary electromagnetic transmission, have been found too. The structures have been manufactured and their behavior measured experimentally, showing good agreement with the numerical results.

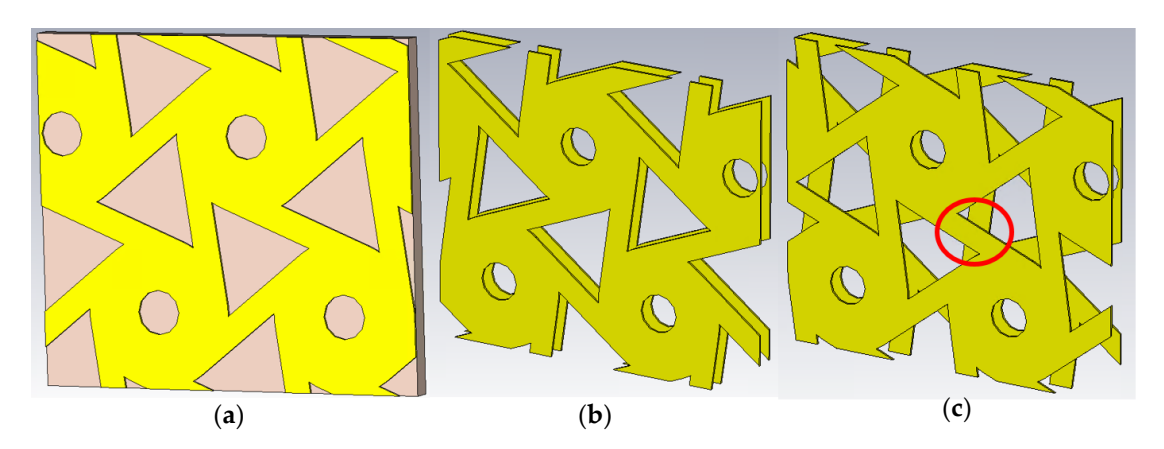


Figure 2. Schematic of the three honeycomb configurations studied in this work: (a) one-layer structure, (b) bilayer non-chiral structure, and (c) bilayer chiral structure. The difference between (b,c) structures is marked in red. In (b,c) the substrate has been removed for a better visualization of the metallic patterns.

2. Numerical Design and Experimental Characterization

As has been mentioned, we have designed several structures using PCB technology with the aid of the commercial electromagnetic simulator Dassault Systèmes Simulia Corp (Providence, Rhode Island, USA) CST Studio SuiteTM. The chosen substrate is a standard Rogers RO4003C ($\epsilon_r = 3.55$ and $tg\delta = 0.0027$ at 10 GHz) board of 60 mils thickness (i.e., 1.524 mm) with a metal cladding of 35 μ m. To experimentally characterize the structure,

Electronics **2025**, 14, 2521 4 of 14

a sample has been manufactured by laser ablation with the aid of an LPKF (Garbsen, Germany) Protolaser S machine. The fabricated sample, shown in Figure 1, is composed of 12×12 unit cells.

The characterization of the structure has been performed within an anechoic chamber, Figure 3, using an Agilent (Santa Clara, California, USA) E8362A PNA Series Network Analyzer (PNA). Two standard gain horn antennas have been used as transmitter and receiver. A sample holder is placed between both antennas; it consists of a metal sheet, covered by absorbent material, which presents a circular hole, of diameter 18 cm, in its central part. The metamaterial sample under test (SUT) is placed in the hole in such a way that the signal reaching the receiving antenna only passes through the metamaterial.

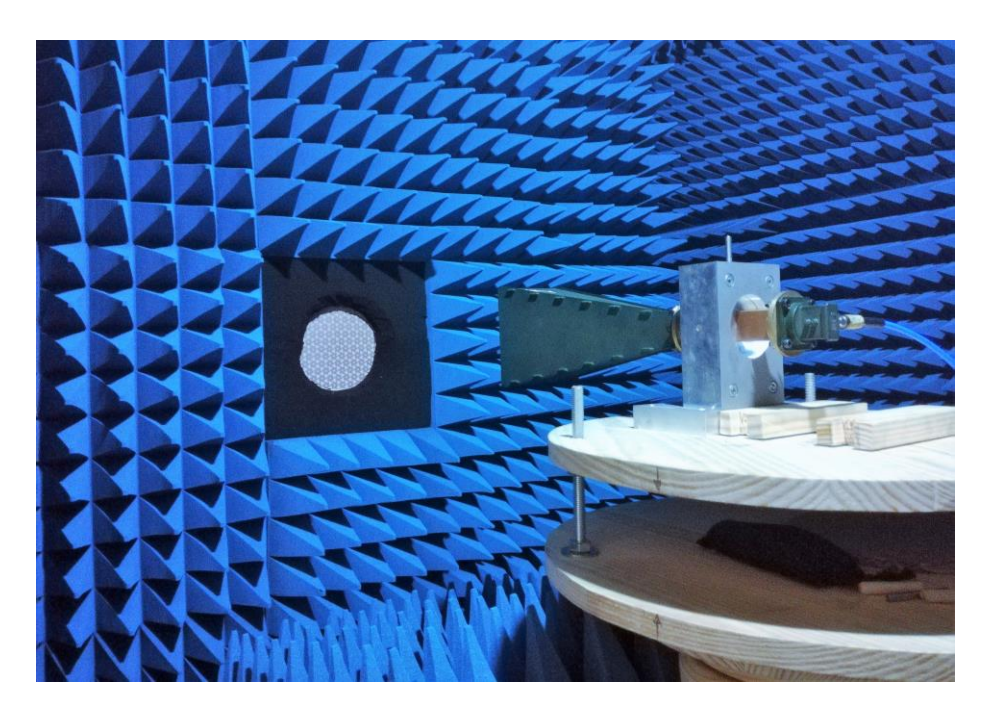


Figure 3. Microwave setup used for the experimental characterization of the structures.

To carry out the characterization of the metamaterial, three types of measurements were made with the aid of the PNA. First, with the SUT placed on the sample holder, the scattering parameters S_{11} and S_{21} (i.e., reflection and transmission coefficients) when both antennas were in co-polar (S_{21Co}^A) and cross-polar ($S_{21Cross}^A$) orientations, were measured. These scattering parameters consider not only the response of the metamaterial but also the response of the propagation channel and the antennas. To obtain the SUT scattering parameters of the co-polar (S_{11Co} and S_{21Co}) and cross-polar ($S_{21Cross}$, in a chiral material $S_{11Cross} = 0$ [1]) components, two reference measurements are needed [30]. In the first one, the SUT is replaced by a conductor plane (copper) and the reflection is measured (S_{11PEC}^A). In the second one, the conductor is removed and the parameter S_{21} is measured with the sample holder empty (S_{21Free}^A). The calibration of the preliminary parameters relative to the reference measurements leads to the desired SUT scattering parameters,

$$S_{21Co} = \frac{S_{21Co}^{A}}{S_{21Free}^{A}} e^{-j\beta d}; S_{21Cross} = \frac{S_{21Cross}^{A}}{S_{21Free}^{A}} e^{-j\beta d}; S_{11Co} = \frac{S_{11Co}^{A}}{S_{11PEC}^{A}} e^{-j\pi}$$
(1)

where β is the phase constant and d the width of the SUT. A time dependence $e^{+j\omega t}$ is assumed.

Electronics **2025**, 14, 2521 5 of 14

3. Results: 2D and 3D Non-Chiral Structures

First, we have numerically studied the response of the honeycomb pattern printed only on one face of the PCB, as shown in Figure 2a. This structure is basically two-dimensional, so, following [4,24] electromagnetic activity should be negligible or, at least, very small.

The scattering parameters for a linearly polarized plane wave with normal incidence are shown in Figure 4. Due to the structure symmetry, the results do not depend on the polarization plane of the incident wave. The frequency response of this single-layer structure is governed by a phenomenon known as extraordinary transmission (ET) [31–33]. With subwavelength apertures, whether the triangles, the circles, or both, the transmission coefficient of this structure presents a bandpass behavior with high transmission. As expected, the transmission peak is followed by a dip, the Wood–Rayleigh (WR) anomaly [33]. The same behavior is observed in our sample: in Figure 4, the period of the structure is d = 16.48 mm, while the WR anomaly happens at 16.86 GHz, i.e., $\lambda = 17.79$ mm; the increase in the pattern period downshifts the anomaly frequency accordingly. Moreover, the larger the aperture size, the lower the central frequency of the passband and the wider its bandwidth.

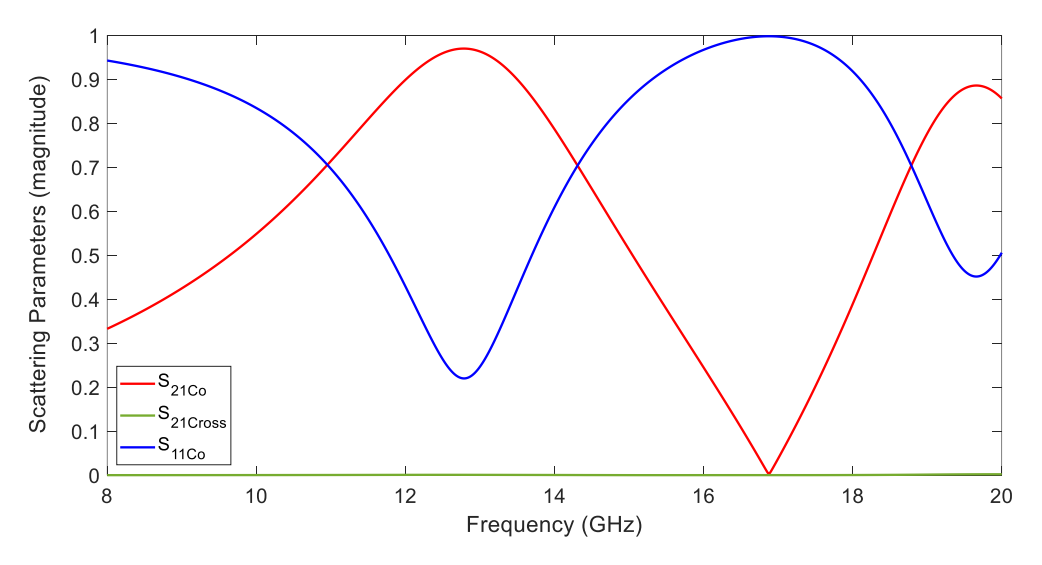


Figure 4. Scattering parameters of the single-layer structure shown in Figure 2a.

Figure 5 presents the electric (a) and magnetic (b) field magnitude distribution in the yz and xz planes, respectively, at the frequency of maximum transmission. It can be observed that the transmitted electric field is originated by the diffraction at the triangular slot edges and thus, near the metamaterial is highly concentrated around these holes. Meanwhile, the magnetic field, Figure 5b, is concentrated surrounding the straight arms that interconnect the hexachiral unit cells. Therefore, as the triangular slots are enlarged, the arms/ribs of the hexachiral structure are narrower so its inductance is also increased, and the resonance frequency is reduced.

Paying attention to the chiral behavior of the structure, Figure 4 shows no cross-polarized parameters, i.e., $S_{11Cross} = S_{21Cross} = 0$, so no gyrotropy (electromagnetic activity) is observed, which is consistent both with the theory and with the experimental results described in [23].

Electronics **2025**, 14, 2521 6 of 14

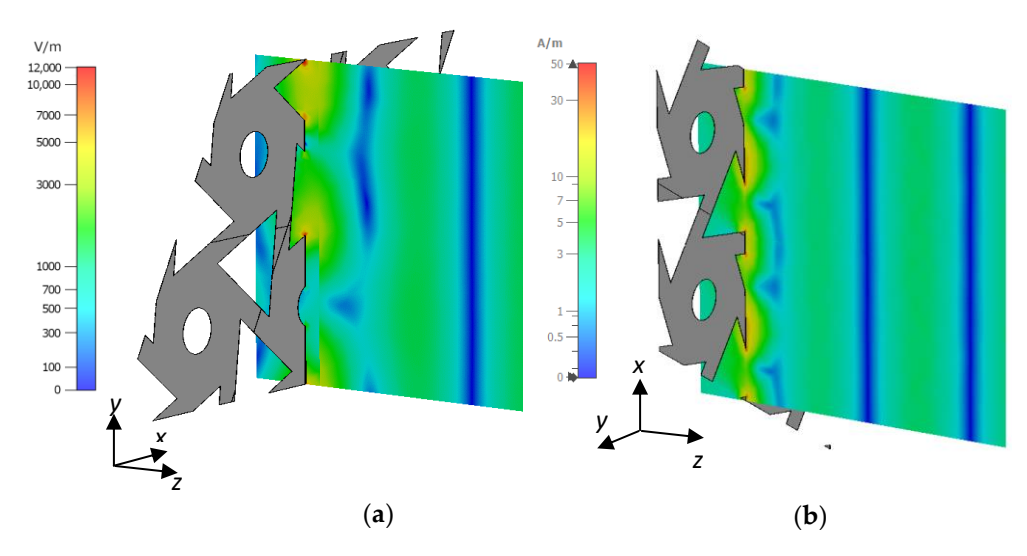


Figure 5. Electromagnetic field at 12.8 GHz. The structure is placed in the xy plane. Dielectric has been removed for better visualization. Color scales are logarithmic. (a) Electric field distribution in yz plane. (b) Magnetic field distribution in xz plane.

Next, after analyzing the single-layer structure with its ET behavior, a two-layer structure, Figure 2b, with the same pattern on both PCB sides, is studied. As in the previous case, this structure has mirror symmetry and, consequently, it should not present electromagnetic activity. The aim of this dual-layer configuration is analyzing the non-chiral resonance between both faces; the effect of the chirality will be studied in the next section. Figure 6 presents the scattering parameters of this stacked structure. Now it can be seen that, in the analyzed frequency range, the S_{21} parameter shows three transmission peaks before the WR anomaly at f_{WR} = 19.6 GHz: a wide one at 14.3 GHz, marked in Figure 6 as B, and two narrower peaks at 9.2 GHz (A) and 18.7 GHz (C). As in the previous case, the cross-polar transmission and reflection, as expected, are negligible. Consequently, we can confirm that there is no observable chiral behavior.

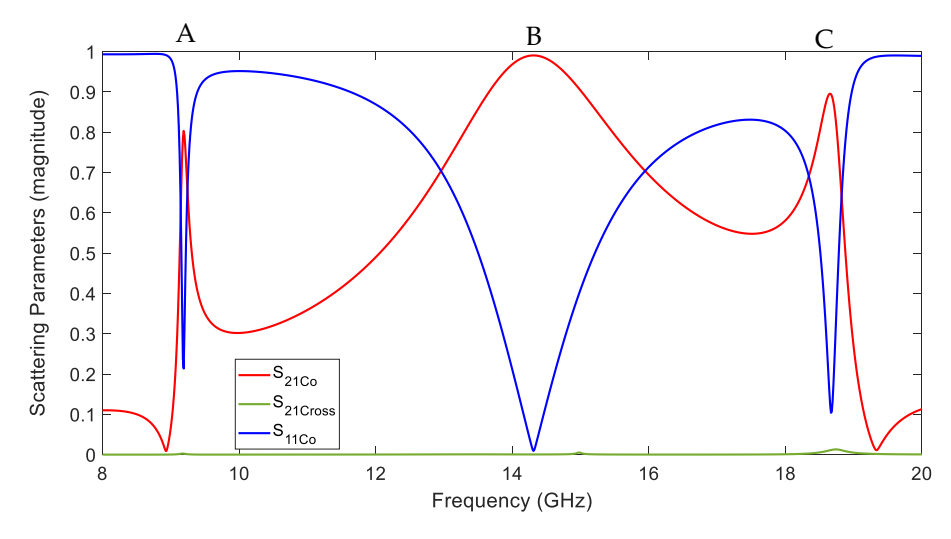


Figure 6. Scattering parameters for a plane wave normally incident on a PCB including two parallel metal layers as shown in Figure 2b. Three transmission maxima (A, B and C) are observed.

The transmission peak B, as the one presented by the single-layer grid (Figure 4), is due to the extraordinary transmission generated by the diffraction at the triangular slot edges. Upon inspection of the electric field distribution at this frequency, shown in Figure 7b, we can observe that, as in the single-layer structure (Figure 5), the electric field is concentrated around the triangles. However, in the dual-layer structure, owing to this stacking of layers,

Electronics **2025**, 14, 2521 7 of 14

the capacitive coupling between them produces higher field magnitude and an upshift in the frequency response, from 12.5 to 14.2 GHz.

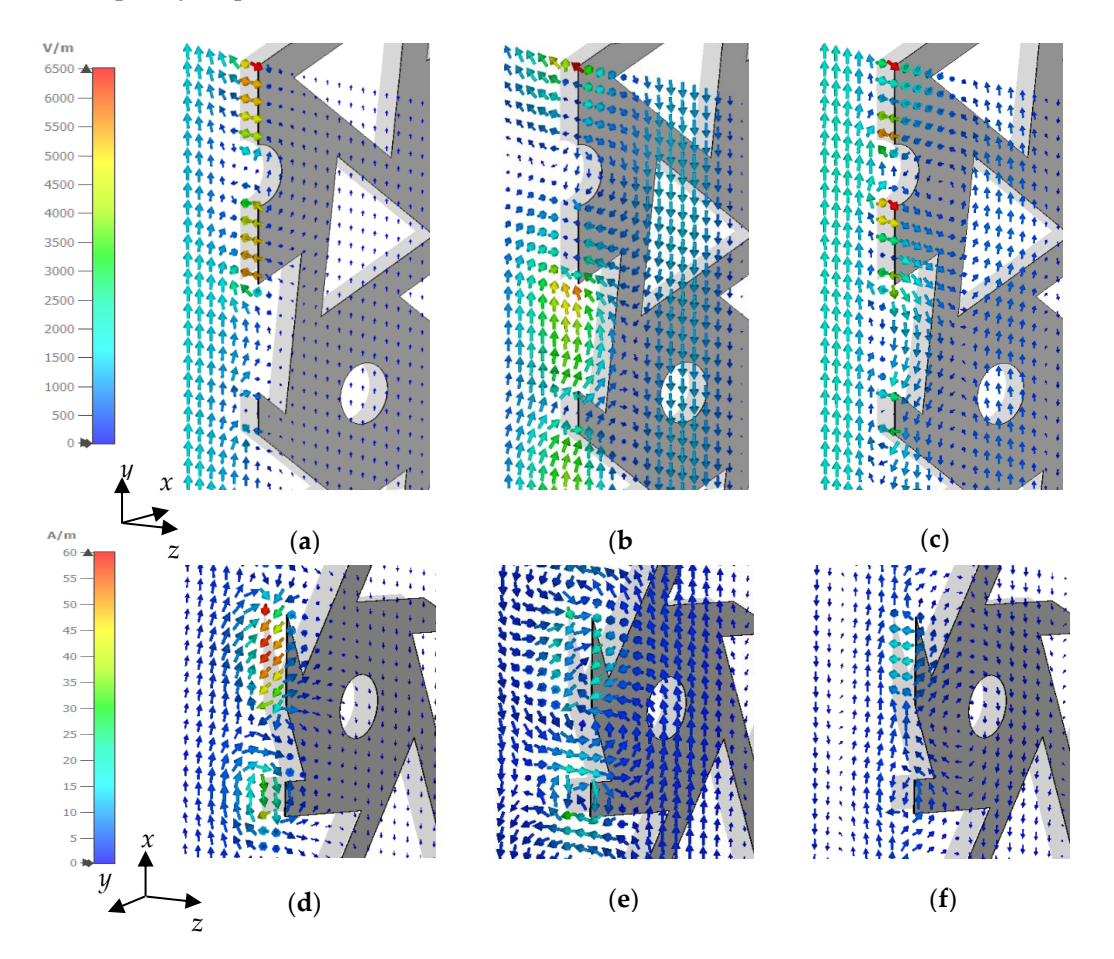


Figure 7. Electric field (yz plane) at different frequencies (the structure is placed in the xy plane): (a) Peak A at 9.2 GHz. (b) Peak B at 14.3 GHz. (c) Peak C at 18.7 GHz. Magnetic field (x-z plane): (d) Peak A. (e) Peak B. (f) Peak C.

Moreover, the transmission peaks, A and C, have different origins. At these frequencies, when a linearly polarized wave impinges on the structure, it induces antiparallel surface currents on both layers. These current distributions provide a high confinement between both metallic layers of the electric (Figure 7a,c) and magnetic (Figure 7d,f) fields, in a comparable way to the results observed in other double-layered fishnet structures [34].

We are going to focus the analysis on transmission peak A, although the analysis and conclusions are also extensible for explaining the transmission peak C. We have represented with arrows in Figure 8a the direction of the currents on both metal layers. It can be observed that the antiparallel currents are induced both in the arms that interconnect the circular crowns and in the crown itself. This current distribution generates a high capacitive coupling between layers, mainly between the circular crowns of the honeycombs (Figure 7a). Analyzing the electric field near the metal layers (Figure 8b), we can observe electric dipole moments both between edges of the circular slot, and between the edges of the triangular slots. Both types of dipoles are oriented parallel to the incident field, but with opposite direction.

Electronics **2025**, 14, 2521 8 of 14

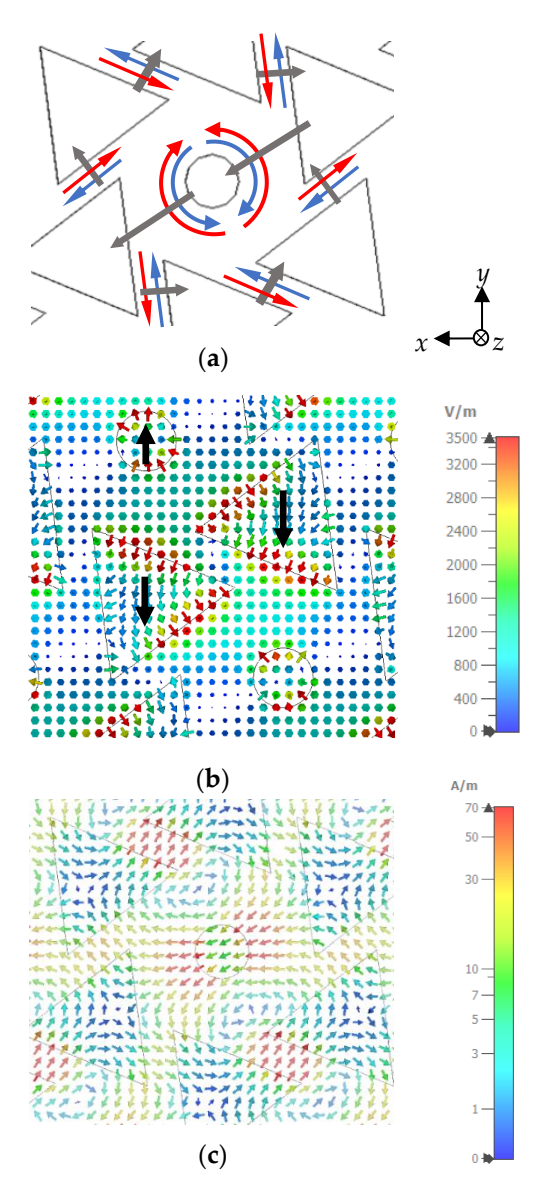


Figure 8. (a) Representation of surface current directions at 9.2 GHz, Ey incidence (red arrows for the current on the top metal layer, blue arrows for the bottom metal layer). The resultant magnetic dipoles are also represented by grey arrows. (b) Electric field distribution in an xy plane near the metallization. (c) Magnetic field distribution in an xy plane in-between both metal layers.

Moreover, these antiparallel currents conform current loops that provide different magnetic dipole moments, represented with grey arrows in Figure 8a, which are responsible for the high magnetic field confinement between the arms of the hexachiral structures of both layers, Figure 7d. This concentration of the magnetic field is represented in more detail in Figure 8c, where the magnetic field distribution in a plane in-between both metal layers is shown. In fact, it can be observed that the magnetic field, Figure 8a, is aligned along these dipole moments created between both layers.

The combination of the radiation of these dipoles produces a scattered electromagnetic field parallel to the incident one, i.e., this structure presents only co-polar transmission, with a negligible cross-polar component.

4. Results: Chiral Structure

In this section we model a third configuration with the aim of providing 3D chirality to the structure. This new structure is composed of two metal layers with the same shape

Electronics **2025**, 14, 2521 9 of 14

and dimensions as in the previous section, but one layer being the specular image of the other one, i.e., the first one turned around, as shown in Figure 2c. With this configuration, the structure is geometrically reciprocal, i.e., identical when observed from both sides, and chiral in 3D space, at least from a geometric point of view.

Figure 9 shows the scattering parameters of the proposed structure (Figure 2c) obtained by means of numerical simulations both at a wide frequency range 1–20 GHz, Figure 9a, and a detail of the X-band where the first resonance occurs, Figure 9b. In this last figure, the numerical results are compared with the experimental ones. The measurements have been performed in X-band, since this is the frequency band where the chiral behavior that was being sought was present.

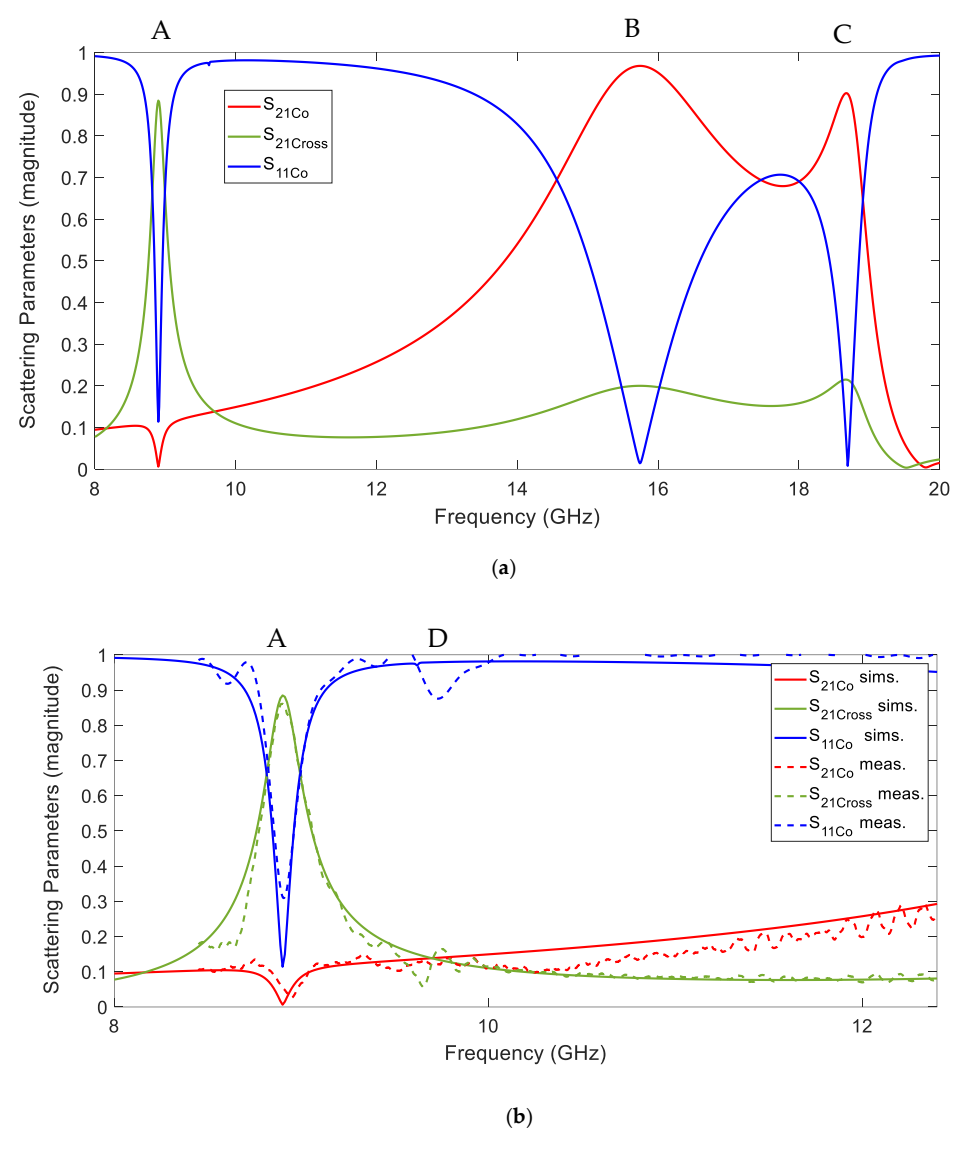


Figure 9. Scattering parameters of the bilayer 3D chiral structure pictured in Figure 2c. (a) Simulation results in 1–20 GHz range. (b) Comparison between numerical and experimental data in X-band. A, B and C are the same transmission peaks found in the bilayer nonchiral structure (Figure 6), a new resonance (D) is found in the experimental results.

On inspecting Figure 9a, we observe a great similarity between the S-parameters (module) of this chiral dual-layer structure and those of the non-chiral one, Figure 6, with three transmission peaks placed at very similar frequencies. The origins of these peaks are the same as in the previous structure: one transmission peak is due to extraordinary transmission and the other two are generated by the resonances between both metal layers.

Electronics **2025**, 14, 2521 10 of 14

However, the main difference is that, in this new case, there is not only co-polarized transmission but also cross-polarized transmission, mainly at the first transmission peak (A). Focusing our attention on this peak, and observing this resonance frequency in detail, Figure 9b, we can observe that the transmission of the co-polar component, S_{21Co} , is almost negligible compared with the high transmission of the cross-polar one, $S_{21Cross}$. Moreover, the comparison between measurements and simulations shows a good agreement between both. At about 0.8 GHz above peak A, the measured results present a small resonance (D) not present in simulations. This issue is due to alignment errors in the measurement setup, with the incident field impinging not totally normal on the metamaterial. In fact, simulations with a deviation of about 2 degrees in the incidence angle showed this second resonance.

From the scattering parameters the chiral behavior of the dual-layer hexachiral structure is analyzed. The polarization plane rotation angle of the transmitted signal is presented in Figure 10. The rotation follows the well-known Condon model [1], with a first resonant frequency at f = 8.7 GHz, i.e., the transmission maximum in Figure 9b. Moreover, the ellipticity is negligible in the whole frequency range, even at the frequency of maximum rotation where it provides very low ellipticity (0.06 in the numerical result and -0.014 when measured experimentally). So, at this frequency, the hexachiral structure presents electromagnetic activity, behaving as a 90 ° polarization rotator without the degradation of the linear polarization thanks to the lack of circular dichroism.

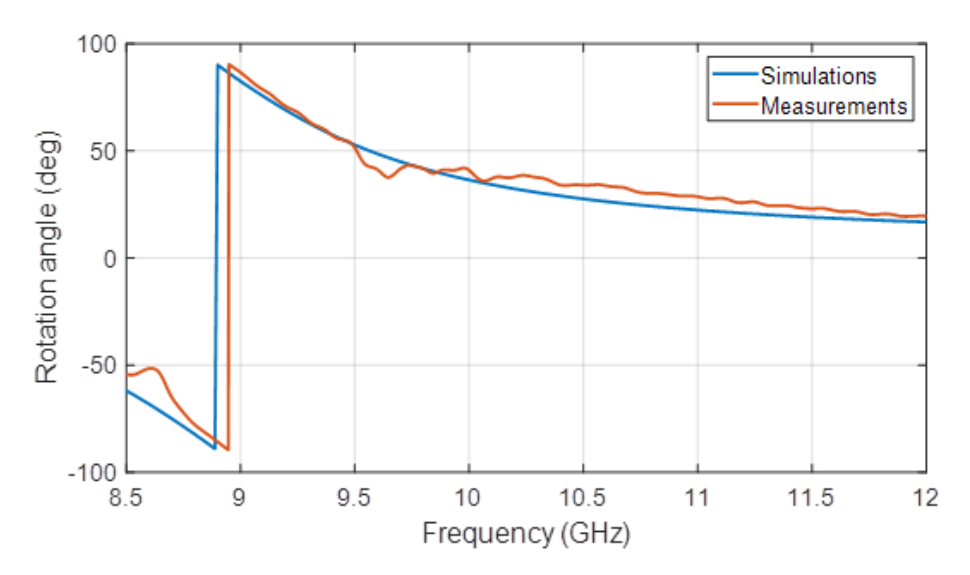


Figure 10. Rotation of the polarization plane (degrees). Simulations solid line, measurements dashed line.

As in the previous dual-layer case, the EM response of the structure can be explained by means of the dipole moments induced on the metal layers. Figure 11 presents the surface currents on both metal layers and the magnetic field distribution at the resonance frequency A.

On inspection of Figure 11a,c, we observe that the currents on both layers form loops that induce different magnetic dipole moments. The most significative current loops are represented with solid/dash arrows and their dipole moments identified as $\overrightarrow{m_1}$, $\overrightarrow{m_2}$, and $\overrightarrow{m_3}$. These dipoles appear not only between the circular crown of the honeycomb, $\overrightarrow{m_3}$, but also on the arms that interconnect the hexachiral structure, $\overrightarrow{m_1}$ and $\overrightarrow{m_2}$. As observed in Figure 11b, these dipoles produce a high magnetic field between both layers. The combination of these dipoles originates the resultant transmitted field. However, in contrast with the previous bilayered structure, in this case, the combination of the hexachiral with its specular image

rotates the magnetic dipoles and, then, the scattered field. This way, an electromagnetic coupling provides the scattering of cross-polar field components H_{ν} and E_{κ} .

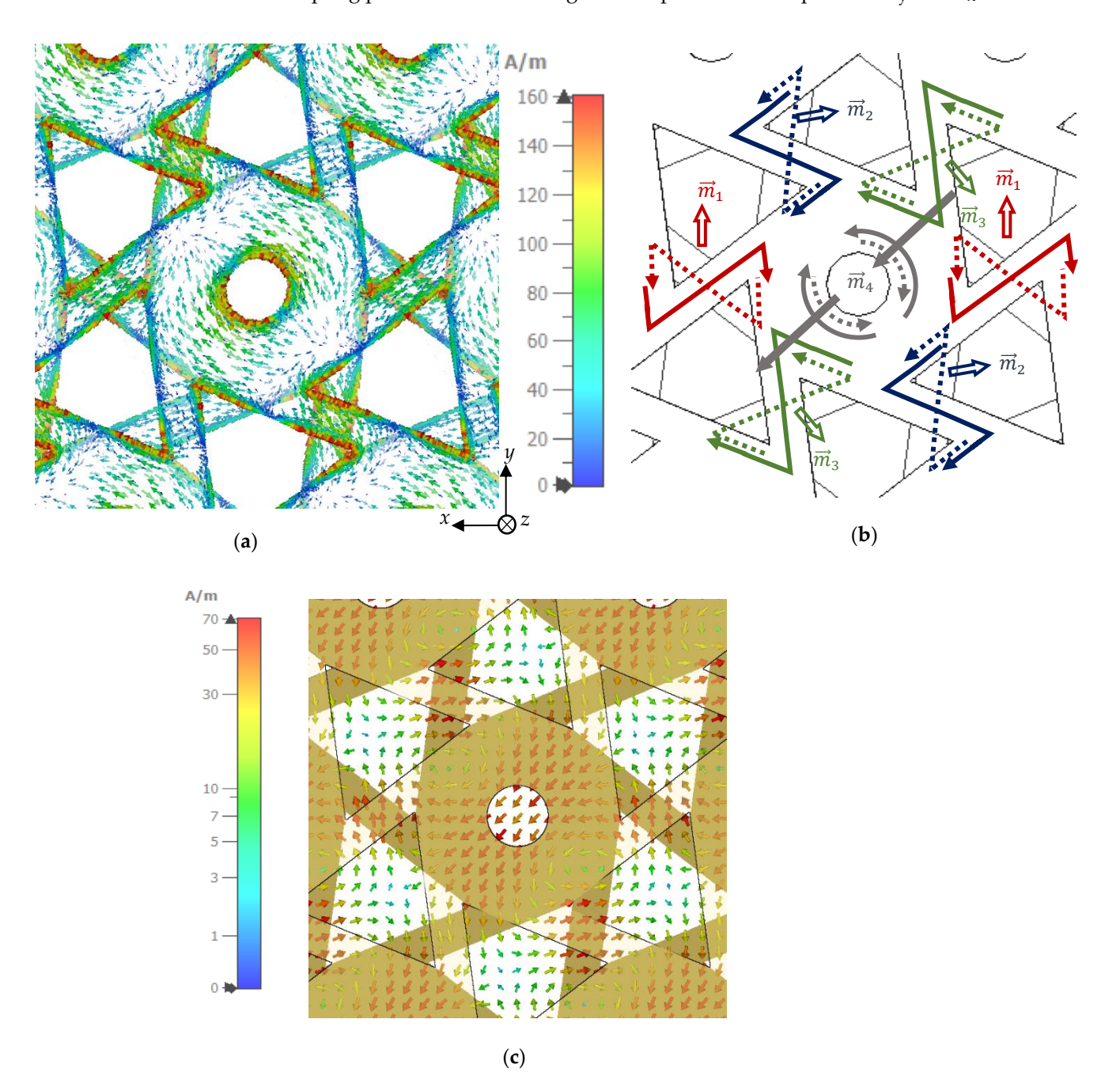


Figure 11. (a) Surface currents on both layers at the A-peak frequency. (b) Representation of current directions: continuous line—top layer (-z) and dashed line—bottom layer (+z). Equivalent magnetic dipoles are also represented (compare with Figure 8). Colors are used to distinguish different dipoles, having no further meaning (c) Magnetic field distribution in a xy plane in-between both metal layers.

In this structure with conjugated faces, the chiral behavior is originated mainly on the arms that interconnect the honeycombs and their mutual orientation, determining the current distribution and thus the orientation of the electric and magnetic dipoles. The width of these arms, geometrical parameter c, influences this distribution; by reducing the thickness of the arms, the dipole moments increase, increasing the transmission of the cross-polar component.

5. Conclusions

In this paper, we have numerically and experimentally analyzed the electromagnetic behavior of a hexachiral metamaterial structure. The proposed structure, based on PCB technology, presents a honeycomb-inspired periodic pattern that leads to an extraordinary transmission at a certain frequency. Moreover, the combination of two layers of the same structure gives rise to additional transmission peaks due to the resonance between both layers. If previous studies with similar structures did not find any sign of electromagnetic activity, we have demonstrated that a bilayered structure indeed presents this behavior when one layer is the specular image of the other one.

Numerical and experimental results are in good agreement and show that the proposed chiral structure presents a strong electromagnetic activity on its first transmission peak. At this frequency, the hexachiral structure behaves as a 90° polarization rotator without polarization distortion. In fact, numerical results show that the energy losses of this structure are lower than 30% of the incident energy, the maximum absorption being coincident with the resonance frequency (peak A, i.e., the frequency where the \pm 90° polarization rotation takes place). As mentioned in the introduction, such structures could then be employed in applications where their mechanical properties are needed, as deployable devices.

Author Contributions: Conceptualization, I.B.; methodology, Ó.F. and I.B.; modeling, I.B.; validation, Ó.F. and Á.G.-G.; writing—original draft preparation, I.B. and Ó.F.; numerical simulations, I.B. and Ó.F.; experimental setup, Á.G.-G. and Ó.F.; measurements, Á.G.-G. and Ó.F.; writing—review and editing, Á.G.-G., A.C.L.-C. and A.G.; visualization, Ó.F.; supervision, Á.G.-G., A.C.L.-C. and A.G.; project administration, I.B., Á.G.-G. and A.C.L.-C.; funding acquisition, I.B., Á.G.-G. and A.C.L.-C. All authors have read and agreed to the published version of the manuscript.

Funding: This research was funded by the Spanish Ministry of Science and the European Union: MCIN/AEI/10.13039/501100011033/FEDER, UE, grant number PID2022-137619NB-I00, and also Projects PGC2018-098350-BC21 and PGC2018-098350-B-C22.

Data Availability Statement: Data are contained within the article.

Acknowledgments: The authors thank S. Pana and M. López, from the University of Cantabria, for her useful work implementing the hexachiral structure and his help in the sample holder design; R.R. Boix and R. Rodríguez-Berral for their comments; M. Beruete for his help with the CST modelling; and G. Molina-Cuberos for his help with the data processing.

Conflicts of Interest: The authors declare no conflicts of interest. The funders had no role in the design of the study; in the collection, analyses, or interpretation of data; in the writing of the manuscript; or in the decision to publish the results.

References

- 1. Lindell, I.V.; Sihvola, A.H.; Tretyakov, S.A.; Viitanen, A.J. *Electromagnetic Waves on Chiral and Bi-Isotropic Media*; Artech House: Boston, MA, USA, 1994.
- 2. Wang, Z.; Cheng, F.; Winsor, T.; Liu, Y. Optical chiral metamaterials: A review of the fundamentals, fabrication methods and applications. *Nanotechnology* **2016**, *27*, 412001. [CrossRef] [PubMed]
- 3. Eleftheriades, G.V.; Balmain, K.G. *Negative Refraction Metamaterials: Fundamental Principles and Applications*; Wiley-IEEE Press: Hoboken, NJ, USA, 2005.
- 4. Barba, I.; Cabeceira, A.C.L.; García-Collado, A.J.; Molina-Cuberos, G.J.; Margineda, J.; Represa, J. Quasi-Planar Chiral Materials for Microwave Frequencies. In *Electromagnetic Waves Propagation in Complex Matter*; Khisk, A., Ed.; Intech: London, UK, 2011.
- 5. Rogacheva, A.V.; Fedotov, V.A.; Schwanecke, A.S.; Zheludev, N.I. Giant Gyrotropy due to Electromagnetic-Field Coupling in a Bilayered Chiral Structure. *Phys. Rev. Lett.* **2006**, 97, 177401. [CrossRef]
- 6. Marqués, R.; Jelinek, J.; Mesa, F. Negative refraction from balanced quasi-planar chiral inclusions. *Microw. Opt. Technol. Lett.* **2007**, 49, 2606–2609. [CrossRef]

7. Zhou, J.; Dong, J.; Wang, W.; Koschny, T.; Kafesaki, M.; Soukoulis, C.M. Negative refractive index due to chirality. *Phys. Rev. B* **2009**, *79*, 121104. [CrossRef]

- 8. Molina-Cuberos, G.J.; García-Collado, Á.J.; Barba, I.; Margineda, J. Chiral metamaterials with negative refractive index composed by an eight-cranks molecule. *IEEE Antennas Wirel. Propag. Lett.* **2011**, *10*, 1488–1490. [CrossRef]
- 9. Chen, M.L.N.; Jian, L.J.; Sha, W.E.I.; Choy, W.C.H.; Itoh, T. Polarization Control by Using Anisotropic 3-D Chiral Structures. *IEEE Trans. Antennas Propag.* **2016**, *64*, 4687–4694. [CrossRef]
- 10. Jia, Y.-P.; Zhang, Y.-L.; Dong, X.-Z.; Zheng, M.-L.; Li, J.; Liu, J.; Zhao, Z.-S.; Duan, X.-M. Complementary chiral metasurface with strong broadband optical activity and enhanced transmission. *Appl. Phys. Lett.* **2014**, *104*, 011108. [CrossRef]
- 11. Decker, M.; Ruther, M.; Kriegler, C.E.; Zhou, J.; Soukoulis, C.M.; Linden, S.; Wegener, M. Strong Optical Activity from Twisted-cross photonic metamaterials. *Opt. Lett.* **2009**, *34*, 2501–2503. [CrossRef]
- 12. Fernández, Ó.; Gómez, A.; Basterrechea, J.; Vegas, A. Reciprocal Circular Polarization Handedness Conversion using Chiral Metamaterials. *IEEE Antennas Wirel. Propag. Lett.* **2017**, *16*, 2307–2310. [CrossRef]
- 13. Zhou, J.; Chowdhury, D.R.; Zhao, R.; Azadm, A.K.; Chen, H.T.; Soukoulis, C.M.; Taylor, A.J.; O'Hara, J.F. Terahertz chiral metamaterials with giant and dynamically tunable optical activity. *Phys. Rev. B* **2012**, *86*, 035448. [CrossRef]
- 14. Chen, H.-T.; O'Hara, J.F.; Taylor, A.J.; Averitt, R.D.; Highstrete, C.; Lee, M.; Padilla, W.J. Complementary Planar Terahertz Metamaterials. *Opt. Express* **2007**, *15*, 1084–1095. [CrossRef] [PubMed]
- 15. Li, Z.; Alici, K.B.; Colak, E.; Ozbay, E. Complementary Chiral metamaterials with giant optical activity and negative refractive index. *Appl. Phys. Lett* **2011**, *98*, 161907. [CrossRef]
- 16. Liu, Y.; Cheng, Y.; Cheng, Z.Z. A numerical parameter study of chiral metamaterial based on complementary U-shaped structure in infrared region. *Opt. -Int. J. Light Electron Opt.* **2014**, 125, 1316–1319. [CrossRef]
- 17. Barba, I.; Grande, A.; López-Cabeceira, A.C.; Represa, J.; Molina-Cuberos, G.J.; Fernández, O.; Gómez, A. A Complementary Chiral Metamaterial with Giant Electromagnetic Activity and Low Losses. In Proceedings of the 7th International Conference on Metamaterials, Photonic Crystals and Plasmonics, META'16, Málaga, Spain, 25–28 July 2016.
- 18. Qi, C.; Jiang, F.; Yang, S. Advanced honeycomb designs for improving mechanical properties: A review. *Compos. Part B Eng.* **2021**, 227, 109393. [CrossRef]
- 19. Seungwoo, L.; Seongnam, K.; Teum-Teum, K.; Yushin, K.; Muhan, C.; Seung, H.L.; Ju-Young, K. Reversible Stretchable and Tunable Terahertz Metamaterials with Wrinkled Layouts. *Adv. Mater.* **2012**, 24, 3491–3497. [CrossRef]
- Wojciechowski, K.W.; Branca, A.C. Negative Poisson ratio in a two-dimensional "isotropic" model. Phys. Rev. A Gen. Phys. 1989, A40, 7222–7225. [CrossRef]
- 21. Montgomery-Liljeroth, E.; Schievano, S.; Burriesci, G. Elastic properties of 2D auxetic honeycomb structures—A review. *Appl. Mater. Today* **2023**, *30*, 101722. [CrossRef]
- 22. David, V.; Nica, I.; Salceanu, A. Electromagnetic absorbers based on chiral honeycomb slab. In Proceedings of the International Symposium on Electromagnetic Compatibility—EMC Europe, Athens, Greece, 11–12 June 2009; pp. 1–4. [CrossRef]
- 23. Kopyt, P.; Damian, R.; Celuch, M.; Ciobanu, R. Dielectric properties of Chiral Honeycombs: Modelling and experiment. *Compos. Sci. Technol.* **2010**, *70*, 1080–1088. [CrossRef]
- 24. Kuwata-Gonokami, M.; Saito, N.; Ino, Y.; Kauranen, M.; Jefimovs, K.; Vallius, T.; Turunen, J.; Svirko, Y. Giant Optical Activity in Quasi-Two-Dimensional Planar Nanostructures. *Phys. Rev. Lett.* **2005**, *95*, 227401. [CrossRef]
- 25. Fedotov, V.A.; Schwanecke, A.S.; Zheludev, N.I.; Khardikov, V.V.; Prosvirnin, S.L. Asymmetric Transmission of Light and Enantiomerically Sensitive Plasmon resonance in Planar Chiral Nanostructures. *Nano Lett.* **2007**, *7*, 1996–1999. [CrossRef]
- Fedotov, V.A.; Mladyonov, P.L.; Prosvirnin, S.L.; Rogacheva, A.V.; Chen, Y.; Zheludev, N.I. Asymmetric Propagation of Electromagnetic Waves through a Planar Chiral Structure. *Phys. Rev. Lett.* 2006, 97, 167401. [CrossRef] [PubMed]
- 27. Zhao, R.; Zhang, J.; Zhou, J.; Koschny, T.; Soukoulis, C.M. Conjugated gammadion chiral metamaterial with uniaxial optical activity and negative refractive index. *Phys. Rev. B* **2011**, *83*, 030515. [CrossRef]
- 28. Barba, I.; Grande, A.; López-Cabeceira, A.C.; Represa, J. A Bi-Isotropic Hexachiral Grid in PCB. In Proceedings of the IEEE MTT-S International Conference on Numerical Electromagnetic Modeling and Optimization for RF, Microwave, and Terahertz Applications—NEMO, Sevilla, Spain, 17–19 May 2017; pp. 254–256. [CrossRef]
- 29. Barba, I.; Grande, A.; Molina-Cuberos, G.; García-Collado, A.J.; Represa, J.; López-Cabeceira, A.C. A Full-Dielectric Chiral Material Based on a Honeycomb Structure. *Int. J. Antennas Propag.* **2018**, 2018, 4198243. [CrossRef]
- 30. Plum, E. Chirality and Metamaterials. Ph.D. Thesis, Optoelectronics Research Centre, University of Southampton, Southampton, UK, 2010.
- 31. Beruete, M.; Sorolla, M.; Campillo, I.; Dolado, J.S.; Martín-Moreno, L.; Bravo-Abad, J.; García-Vidal, F.J. Enhanced Millimeter Wave Transmission Through Quasioptical Subwavelength Perforated Plates. *IEEE Trans. Antennas Propag.* 2005, 53, 1897–1903. [CrossRef]
- 32. Ebbesen, T.W.; Lezec, H.J.; Ghaemi, H.F.; Thio, T.; Wolff, P.A. Extraordinary optical transmission through sub-wavelength hole arrays. *Nature* **1998**, *391*, 667–669. [CrossRef]

33. Medina, F.; Mesa, F.; Marqués, R. Extraordinary Transmission Through Arrays of Electrically Small Holes from a Circuit Theory Perspective. *IEEE Trans. Microw. Theory Tech.* **2008**, *56*, 3108–3120. [CrossRef]

34. Torres, V.; Rodríguez-Ulibarri, P.; Navarro-Cía, M.; Beruete, M. Fishnet metamaterial from an equivalent circuit perspective. *Appl. Phys. Lett.* **2012**, *101*, 244101. [CrossRef]

Disclaimer/Publisher's Note: The statements, opinions and data contained in all publications are solely those of the individual author(s) and contributor(s) and not of MDPI and/or the editor(s). MDPI and/or the editor(s) disclaim responsibility for any injury to people or property resulting from any ideas, methods, instructions or products referred to in the content.